water

MDPI

*Article*

# Landscape Ecological Risk Assessment of Kriya River Basin in Xinjiang and Its Multi-Scenario Simulation Analysis

**Jinbao Li [1,2], Xuemin He [1,2,3,*], Pengcheng Huang [1,2], Zizheng Wang [1,2] and Ranran Wang [1,2]**

[1] College of Ecology and Environment, Xinjiang University, Urumqi 830017, China; 15701919668@163.com (J.L.); wzz952580616@163.com (Z.W.)
[2] Key Laboratory of Oasis Ecology of Education Ministry, Xinjiang University, Urumqi 830017, China
[3] Xinjiang Jinghe Observation and Research Station of Temperate Desert Ecosystem, Ministry of Education, Jinghe 833300, China
* Correspondence: hxm@xju.edu.cn

**Abstract:** To comprehend the potential impacts of both natural phenomena and human activities on ecological risk, a thorough examination of the spatial and temporal evolution characteristics of Landscape Ecological Risk (LER) in arid river basins is imperative. This investigation holds paramount importance for the proactive prevention and mitigation of LER, as well as for the preservation of ecological security within these basins. In this scholarly inquiry, the Kriya River Basin (KRB) serves as the focal point of analysis. Leveraging three historical land use and land cover (LULC) images and incorporating a diverse array of drivers, encompassing both natural and anthropogenic factors, the study employs the PLUS model to forecast the characteristics of LULC changes within the basin under three distinct scenarios projected for the year 2030. Concurrently, the research quantitatively assesses the ecological risks of the basin through the adoption of the Landscape Ecological Risk Assessment (LERA) methodology and the Spatial Character Analysis (SCA) methodology. The results showed the following: (1) The study area is primarily composed of grassland and unused land, which collectively account for over 97% of the total land. However, there has been a noticeable rise in cropland and considerable deterioration in grassland between 2000 and 2020. The key observed change in LULC involves the transformation of grassland and unused land into cropland, forest, and construction land. (2) The overall LER indices for 2000, 2010, and 2020 are 0.1721, 0.1714, and 0.16696, respectively, showing strong positive spatial correlations and increasing autocorrelations over time. (3) Over time, human activities have come to exert a greater influence on LER compared to natural factors between 2000 and 2020. (4) In the natural development scenario (NDS), cropland protection scenario (CPS), and ecological priority scenario (EPS), the LER of KRB experienced notable variations in the diverse 2030 scenarios. Notably, the CPS exhibited the highest proportion of low-risk areas, whereas Daryaboyi emerged as the focal point of maximum vulnerability. These findings offer theoretical and scientific support for sustainable development planning in the watershed.

**Keywords:** Landscape Ecological Risk (LER); Kriya River Basin (KRB); PLUS model; multi-scenario simulation; driving factors



**Citation:** Li, J.; He, X.; Huang, P.; Wang, Z.; Wang, R. Landscape Ecological Risk Assessment of Kriya River Basin in Xinjiang and Its Multi-Scenario Simulation Analysis. *Water* **2023**, *15*, 4256. https://doi.org/10.3390/w15244256

Academic Editors: Richard Smardon and Roko Andricevic

Received: 15 October 2023
Revised: 1 December 2023
Accepted: 9 December 2023
Published: 12 December 2023



## 1. Introduction

Watersheds are geographical areas with complex structures consisting of multiple systems, including ecological, economic, and social, with different functions, such as maintaining biodiversity and supporting human production, life, and culture [1–3]. Global climate change is becoming more pronounced as human activities intensify, and this, combined with the sensitivity and vulnerability of drylands themselves, makes them one of the most ecologically risky regions [4–6]. On the other hand, the rapid expansion of cities has caused enormous ecological and ecological problems, such as the degradation of land resources, the reduction in regional biodiversity, the reduction in the carrying capacity

of the environment and the exacerbation of the problem of ecological security, which is evident in the drylands [7–10]. Arid zones, which are mostly composed of oasis cities and desert ecosystems, have stronger feedback to human activities, which makes them an ideal area for the study of nature–human complex systems [9,11]. In the midst of climate warming and transitional resource exploitation, the high intensity of LULC has brought great pressure on the environment [10]. Consequently, the quantification of ecological risks in a scientific and rational manner, along with the analysis of the drivers responsible for their spatial and temporal variations, has emerged as a prominent focus in ecological and environmental research [12–14].

LERA is an important part of ecological risk assessment, which complements and expands ecological risk assessment [15], and emphasizes the comprehensive analysis of the possible impacts of various large-scale disasters that the regional ecological environment may face [16,17]. LER can be used to evaluate various traditional ecological risk assessment methods, based on the perspective of the coupled association of ecological processes and spatial patterns in landscape ecology, paying more attention to the spatial and temporal heterogeneity of ecological risk and the possible adverse consequences of scale effects, and belonging to an important branch of regional ecological risk assessment [18,19].

The ecological risk assessment method, which is based on the LULC LER, can be used to assess the ecological status of a watershed from both an ecological and landscape perspective [17,20,21]. The method is able to map the interactions between landscape patterns and ecological processes and focuses on describing the spatial and temporal variability of ecological risk, the impact of the spatial distribution of landscape components on ecological risk, and these three areas [22,23]. Thus, from the standpoint of landscape pattern ecological processes, the study of regional ecological security has emerged [24–28]. In the 1990s, Heggem et al. (2000) [29] introduced a landscape pattern analysis approach to assess the impact of human activities on ecological change in watersheds. Later, Kapustka et al. (2001) [30] and other landscape ecology theories introduced ecological risk assessment and used it to propose control strategies. Paukert et al. (2011) [31] evaluated the ecological health of the Colorado River Basin using an LERI constructed using the landscape index method. Research on LER is increasing again both at home and abroad as we enter the 21st century, and most of the evaluation objects are ecologically fragile and sensitive areas as well as areas with high intensity of human activities, which are mainly centered around watersheds, cities, mines, nature reserves, and ecologically fragile areas [23,32–36]. The methods of evaluation include landscape pattern index method [9], entropy value method [37], exposure–response method [38], etc.; additionally, the evaluation scale evolves from a single scale to multiple scales, and numerous researchers have looked into the LER's multi-scale changes [39].

Simulating and forecasting dynamic trends under different conditions is imperative, as is looking into the characteristics of the temporal and spatial evolution of LER in rapidly developing watersheds. Furthermore, in order to support future high-quality economic and social development in watersheds, strategies for optimizing LULC structure in arid watersheds must be proposed [40,41]. Multi-scenario LULC change models can be classified into quantitative predictive models, spatial predictive models and coupled models [36]. Currently, commonly used quantitative forecasting models include Markov, system dynamics (SDs), grey forecasting models (GMs), and artificial neural network (ANN) models [42,43]. Spatial prediction models include the CA model, the CLUE model, and the FLUS model [44–46]. By combining data prediction models and spatial prediction models into a coupled model, the requirements of quantitative and spatial accuracy can be highly met. Liang et al. developed a preamble model called the Patch-Level LULC Simulation (PLUS) model was created [47]. It proposes a rule mining framework based on the Land Expansion Analysis Strategy (LEAS) and CA based on muti-type random patch seeds (CARSs) that can be used to explore the drivers of multiple types of land expansion to determine and predict the patch-level development of the LULC landscape, leading to more accurate LULC simulation results [9,35].

The Keriya River Basin (KRB) is an area with important ecological functions in the north-west arid zone, which is of great significance for regional ecological security as well as water resource protection. The basin is located in the hinterland of the Eurasian continent, far from the sea, with the Taklamakan Desert in the north and the Kunlun Mountains in the south, which makes the basin's climate arid due to its unique geographical location. In recent years, with the increase in population and the demand for economic development, a large amount of land has been reclaimed in the middle and lower plains of the basin, resulting in the evolution from desert land to oases. The main water resources in the basin are composed of surface water and groundwater, but the spatial and temporal distribution of water resources is extremely uneven, and seasonal water shortages often occur in the oases, which leads to constraints on agricultural production [48]. In this context, it is particularly important to effectively assess ecological risks. Based on the LULC of the KRB in 2000, 2010, and 2020, this study analyzes the changing characteristics of landscape types, examines the spatial and temporal evolution of LER, and simulates the development trend of LER of the KRB in three different scenarios using the PLUS model and presents the scenarios of ecological environmental protection, aiming to solve the three practical problems of development and ecological protection of KRB: (1) How did the spatial pattern of LULC in the KRB change from 2000 to 2020? (2) What were the characteristics of the spatial distribution and changes in the LER in the basin, and what are the dominant factors leading to the changes of LER? (3) Which development scenarios optimize ecological risk in catchments?

## 2. Materials and Methods

### *2.1. Study Area*

The Keriya River Basin (KRB), located in the heart of the Eurasian continent, is flanked by the Taklamakan Desert to the north and the Kunlun Mountains to the south (refer to Figure 1). Its geographical coordinates range from 80°09′ to 83°51′ E longitude and 35°14′ to 39°29′ N latitude, encompassing a land area of $70.5 \times 10^4$ km$^2$. The basin is characterized by a warm temperate inland arid desert climate, marked by an average annual temperature of 11.6 °C, a scant annual rainfall of 44.7 mm, and considerable evaporation totaling 2500 mm [49]. The elevation variance from north to south is approximately 5000 m, creating a sloping terrain with higher elevations in the south and lower elevations in the north. Geological tectonics have shaped five distinct landforms in the region: mid-altitude mountains in the upper reaches, pre-mountainous hills in the upper and middle reaches, pre-mountainous sloping plains in the middle and lower reaches, alluvial plains in the lower reaches, and the desert area. These have given rise to a natural desert oasis known as the Daryabuyi Oasis. The area exhibits a typical arid continental climate, with scanty annual precipitation of 44.7 mm, high evaporation of 2500 mm, and predominantly drought-resistant vegetation, Poor vegetation conditions. The central plain serves as the primary agricultural zone, cultivating crops such as cotton, maize, and wheat.

### *2.2. Data Acquisition*

LULC data were obtained from the Globeland30 global land cover database (http://globeland30.org, accessed on 23 April 2023). The dataset encompasses three distinct time periods, namely 2000, 2010, and 2020, and possesses a spatial resolution of 30 m × 30 m [50] that reclassified the LULC into six categories, including: cropland, forest, grassland, water, unused land, and construction land. Data on soil type, GDP, population, temperature, and precipitation are available in the Scientific Data Center for Resources and Environment of Chinese Science (https://www.resdc.cn/, accessed on 16 May 2023). The distance variable was retrieved from OpenStreetMap (https://www.openstreetmap.org/, accessed on 24 May 2023). The patterns of the distance variables were also ascertained. The Euclidean distance analysis also revealed the patterns of the distance variables The DEM data were obtained from the geospatial data cloud (https://www.gscloud.cn/, accessed on 3 May

2023) at a resolution of 30 m. The slope, slope direction, and topographic relief data were calculated through the ArcGIS 10.7 platform.

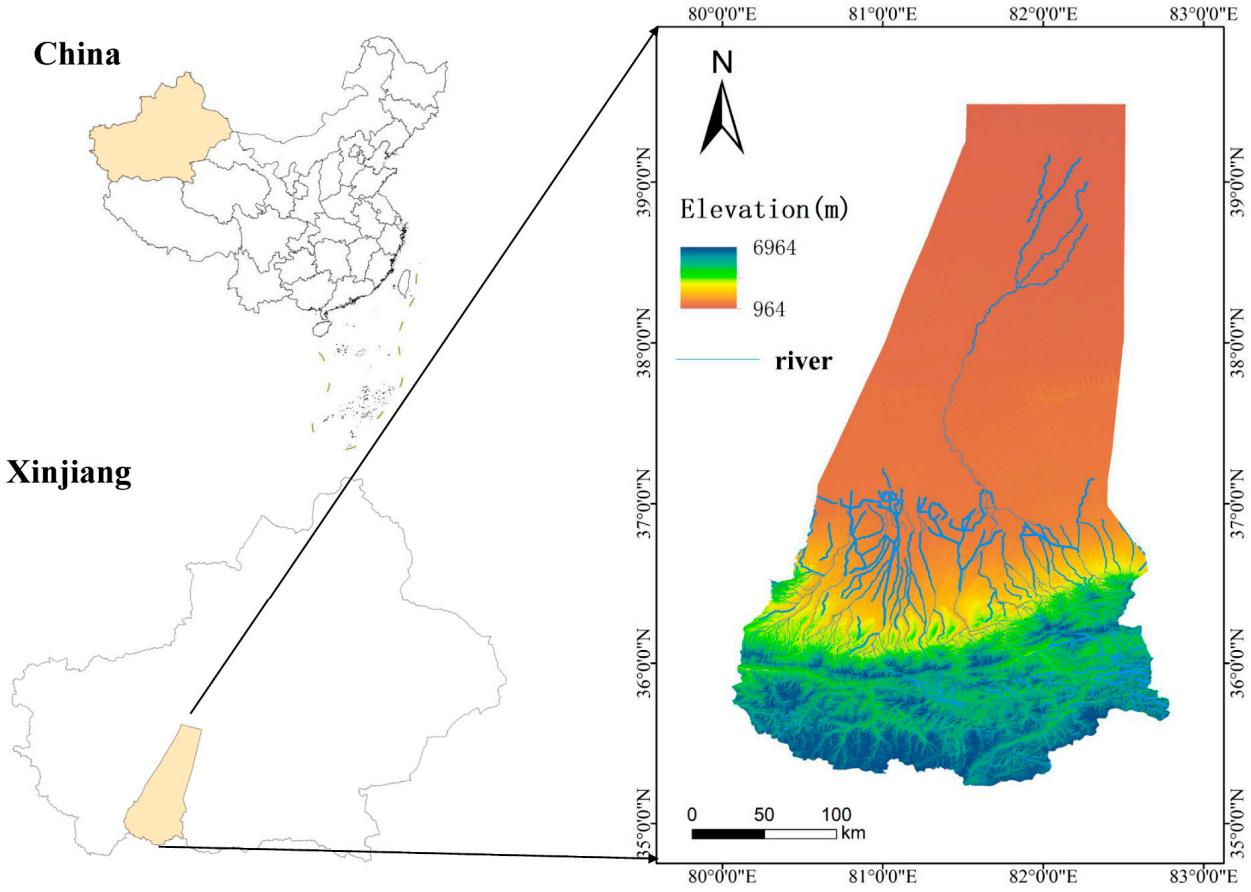


**Figure 1.** Area of study.

### *2.3. Landscape Ecological Risk Index*

This study investigates the spatial and temporal changes in LULC within the KRB region from 2000 to 2020. The analysis combines the PLUS model with five natural and socioeconomic drivers to simulate different scenarios for 2030, including natural development, agricultural land protection, and ecological priority. The regional ecological risk level was quantified using the LERI. The study's methodology and framework are illustrated in Figure 2.

Building upon previous research, this study develops a rating system for the LERI by incorporating landscape disturbance and vulnerability factors [9], and the landscape type index was determined using Fragstats 4.2 software [51]. The LERI was calculated as follows:

$$ERI_i = \sum_{i=1}^{n} \frac{A_{ki}}{A_k} R_i \quad (1)$$

$ERI_i$ is LERI within the ith sampling unit; $A_{ki}$ is the area of landscape type i in the kth sampling unit; $A_K$ is the area of the i-th sampling unit; $R_i$ is the landscape loss degree index.

$$R_i = \sqrt{E_i \times F_i} \quad (2)$$

$$E_i = aC_i + bS_i + cD_i \quad (3)$$

$E_i$ represents the landscape disturbance index, which is constructed by the landscape fragmentation $C_i$, landscape separation $S_i$, and landscape dominance $D_i$, while a, b, and

c denote the weights of the corresponding landscape indexes, and a + b + c = 1. These weights, according to existing research and the actual situation [17,18,52], are assigned as 0.5, 0.3, and 0.2, respectively. Additionally, $F_i$ represents the landscape vulnerability index, and for the six land types of (cropland forest, grassland, watershed, construction land, and unused land), the assigned weights are 0.1905, 0.1429, 0.0952, 0.2381, 0.0476, and 0.2857, based on the characteristics of the study area and the results of previous research [53,54].

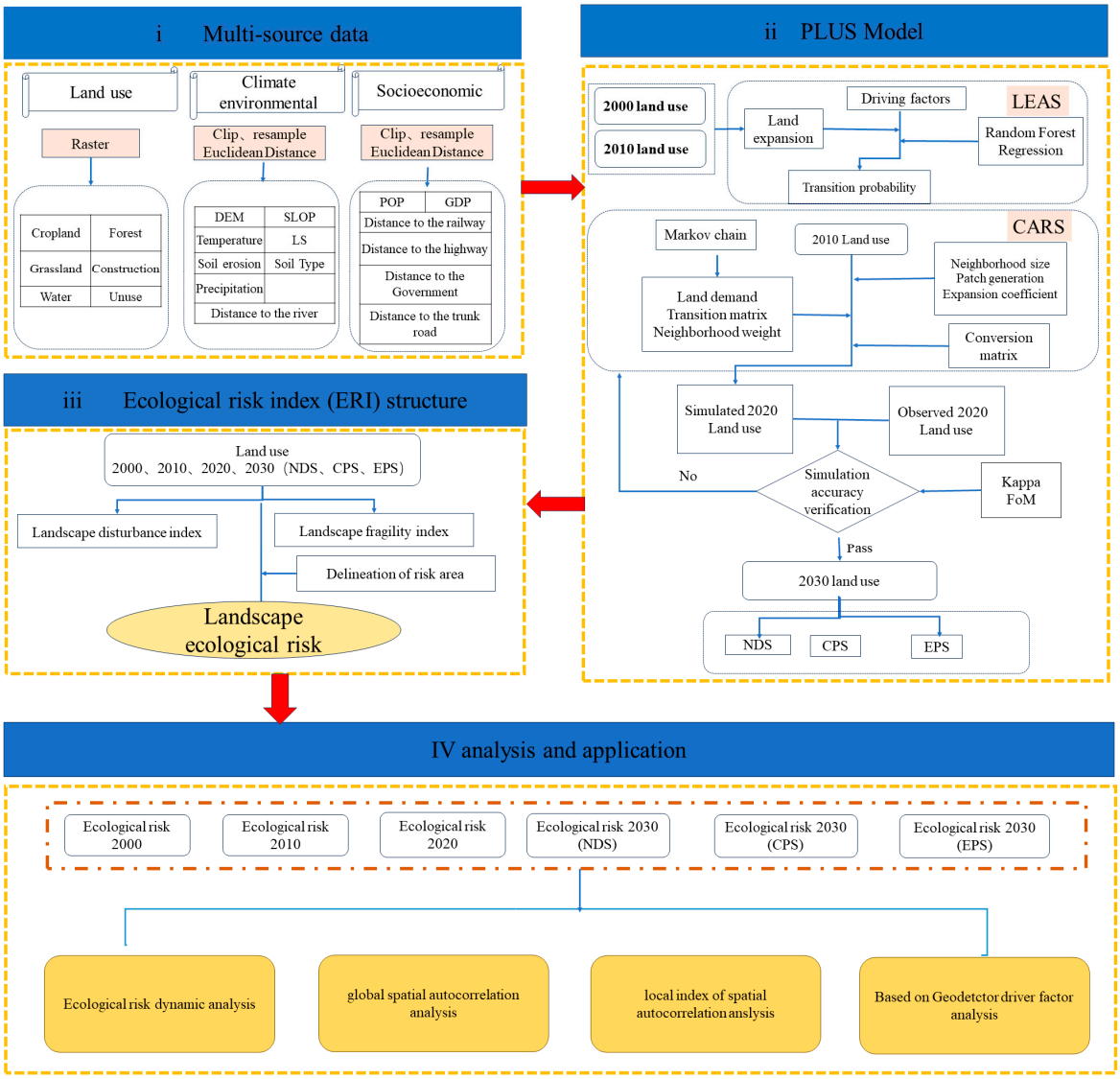


**Figure 2.** Ecological risk assessment framework. PLUS Model: patch-generating land use simulation.

In order to visually analyze the characteristics of spatial distribution of ecological risks, ordinary Kriging interpolation in the geostatistics module of GIS was used to obtain the LER distribution of KRB. The natural breakpoint method was also used to divide the 2020 Landscape Ecological Risk values into five classes: lowest risk (LER < 0.1517), lower risk (0.1517 ≤ LER < 0.2039), medium risk (0.2039 ≤ LER < 0.2846), high risk (0.2846 ≤ LER < 0.3764), and highest risk (0.3764 < LER). The data for the remaining periods were standardized using the 2020 assessment intervals for better comparability.

### *2.4. Analysis of Spatial Autocorrelation for the LER*

Spatial autocorrelation analysis is employed to examine the presence of significant correlations in the spatial distribution of LER. This analysis involves two types of indices: the global Moran's I index evaluates the spatial correlation of attribute values across the

entire study area, while the local Moran's I index assesses the correlation between LER and neighboring spatial units. Moran's I shows a positive correlation when its value is positive, with increasing significance as the value increases. The LISA map is utilized to identify distinct patterns of high–high and low–low clustering of LER within local areas [17,55].

### *2.5. Analysis of the LER Driving Mechanism GeoDetector*

Geographic probes are statistical methods that reveal spatial heterogeneity and, consequently, its driving factors [56]. With reference to related studies, the topographic and climatic characteristics and socioeconomic development of the KRB were also combined to analyze the driving forces of LER changes in the KRB by selecting the following 10 influencing factors from natural and social factors: slope, elevation, climate factors include soil type, annual precipitation, average temperature, distance from a river, GDP, population density, and distance from residential areas [35].

$$q = 1 - \frac{\sum_{h=1}^{L} A_h \sigma_h^2}{A_\sigma^2} \quad (4)$$

In the equation, the $q$ value represents the influence of the driving factor on the LER of the KRB. It ranges between 0 and 1, where a larger $q$-value indicates a stronger explanation of the spatial distribution of the factor on LER. The variable h (1, 2, . . ., $L$) represents the number of subregions of the detection factor X. $A_h$ represents the unit count of layer $h$, and $A$ represents the total area $\sigma_h^2$ denotes the variance of the h layer, while $\sigma^2$ represents the overall variance of the entire region.

### *2.6. Multi-Scenario Ecological Risk Prediction Using the Markov-PLUS Model*

The PLUS model uses a number of steps to analyze changes in LULC. The LULC data are initially transformed into the appropriate format. The expansion proportion of LULC is then extracted using the LEAS module in two stages. Natural and socioeconomic drivers are integrated into the model, and the random forest classification algorithm is employed to determine the driving contribution rate of each driver. This information is then used to calculate LULC change and determine the expansion potential for each LULC type [47]; the Markov model is used to predict the demand of each LULC in 2030, and the panels are automatically generated to acquire the future LULC simulation map in the CARS module [57].

To further investigate the alterations in ecological risk due to different developmental trends in future, this research presents three scenarios: NDS, CPS, and EPS. NDS: The rate of change between 2010 and 2020 is used as a reference to forecast land usage demand in 2030. CPS: Protect cropland by preventing it from being converted to any other LULC type, except for construction land, all other LULC can be converted to cropland. EPS: Preserve forested land and watersheds by prohibiting their conversion to any other LULC. The cost settings for every situation are illustrated in Table 1 underneath.

**Table 1.** Cost matrix for land use conversion in each scenario.

| | **NDS** | | | | | | **CPS** | | | | | | **EPS** | | | | | |
|---|---|---|---|---|---|---|---|---|---|---|---|---|---|---|---|---|---|---|
| 2000–2030 | a | b | c | d | e | f | a | b | c | d | e | f | a | b | c | d | e | f |
| a | 1 | 1 | 1 | 1 | 1 | 1 | 1 | 0 | 0 | 0 | 0 | 0 | 1 | 1 | 1 | 1 | 1 | 1 |
| b | 1 | 1 | 1 | 1 | 1 | 1 | 1 | 1 | 1 | 0 | 1 | 1 | 0 | 1 | 0 | 0 | 0 | 0 |
| c | 1 | 1 | 1 | 1 | 1 | 1 | 1 | 1 | 1 | 1 | 1 | 1 | 0 | 1 | 1 | 1 | 0 | 0 |
| d | 1 | 1 | 1 | 1 | 1 | 1 | 1 | 0 | 1 | 1 | 1 | 1 | 0 | 0 | 0 | 1 | 0 | 0 |
| e | 0 | 0 | 0 | 0 | 1 | 0 | 0 | 0 | 0 | 0 | 0 | 0 | 0 | 0 | 0 | 0 | 1 | 0 |
| f | 1 | 1 | 1 | 1 | 1 | 1 | 1 | 1 | 1 | 1 | 1 | 1 | 1 | 1 | 1 | 1 | 1 | 1 |

Notes: a, b, c, d, e, and f represent cropland, forest, grassland, water, construction land, and unused, respectively, and 0 means no conversion was allowed and 1 means conversion was allowed.

Accuracy Verification

This study uses the 2010 LULC, driving factor data, and LULC extension analysis data as its raw inputs in order to keep the simulation error at a level that is reassuringly acceptable. By contrasting it with the predicted outcomes from the 2020 PLUS model, the accuracy of the spatial distribution of LULC in the study area for the year 2020 is assessed. The assessment of simulation accuracy in this article employs the Kappa coefficient and the Fom coefficient [35,58]. The kappa coefficient, which ranges from 0 to 1, is used to assess the consistency and accuracy of the simulation results. A value greater than 0.7 indicates a higher level of consistency and accuracy. Conversely, the FOM coefficient is computed as the ratio of the intersection of the projected and actual land changes to the total of the two. Higher values of this coefficient, which likewise has a range of 0 to 1, denote increased simulation accuracy [36,59].

## 3. Results

### *3.1. Spatiotemporal LULC Change*

Figure 3 and Table 2 show the spatial and temporal changes in the composition of the six LULC types in the KRB. The overall change in the area of LULC types in the KRB from 2000 to 2020 is more obvious, with unused land and grassland being the most important land types, accounting for more than 78% and 19% of the total land area at all times, respectively, showing a gradually decreasing trend. Arable land, water catchment areas, forest areas, and construction areas generally show increasing trends. In 2000–2020, cropland area continued to increase, with the cropland area increasing by 354.88 km$^2$ and the unused area increasing by 45.51 km$^2$. During 2010–2020, construction land grew the fastest, with an expansion rate of 172%. The distribution of construction land is usually surrounded by cultivated land, which represents the main area of human activity and is subject to the most human intervention. The amount of undeveloped land and grassland will drop by 425.42 km$^2$ and 51.43 km$^2$, respectively, between 2000 and 2020, while the area of water will hardly change.

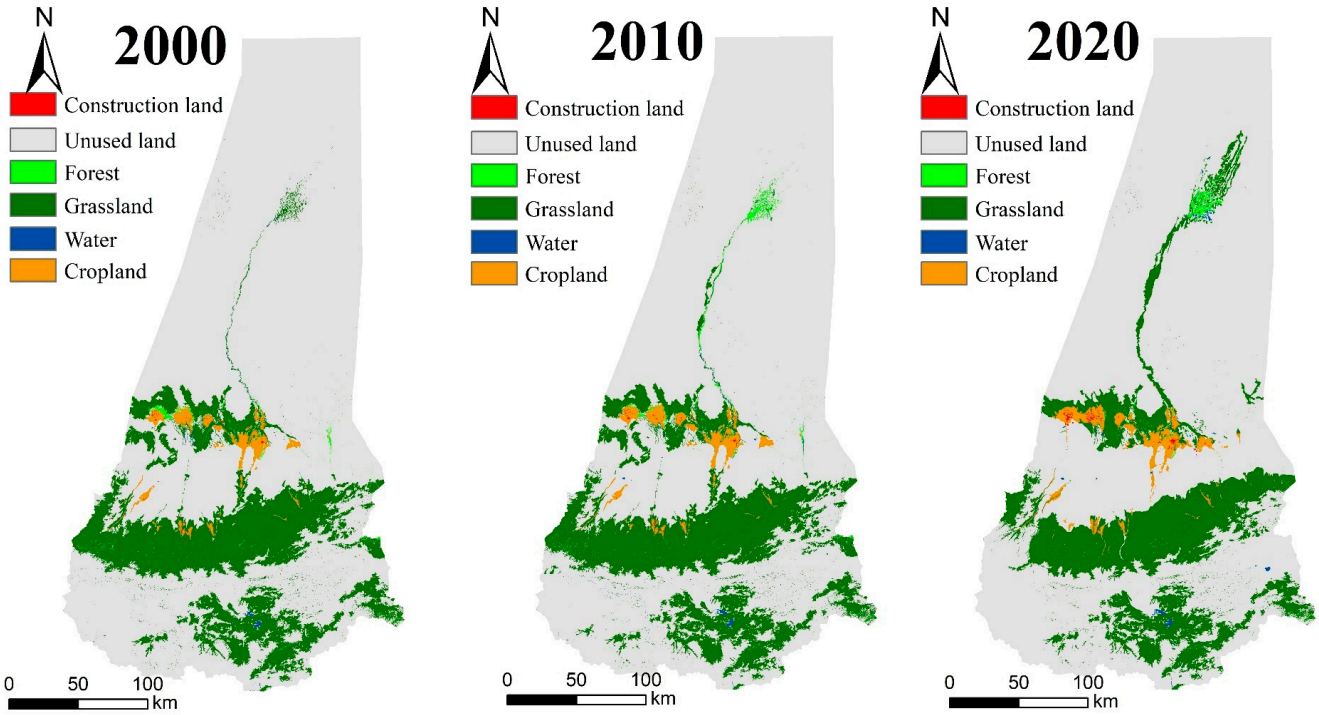


**Figure 3.** Map of LULC in KRB.

**Table 2.** LULC in KRB by area and percentages in 2000, 2010, and 2020.

| Land Use Type | 2000 | | 2010 | | 2020 | |
|---|---|---|---|---|---|---|
| | Area ($km^2$) | Proportion of Total Area (%) | Area ($km^2$) | Proportion of Total Area (%) | Area ($km^2$) | Proportion of Total Area (%) |
| Cropland | 872.8434 | 1.24 | 967.9833 | 1.37 | 1227.725 | 1.74 |
| Forest | 214.4655 | 0.30 | 364.6845 | 0.52 | 265.6377 | 0.38 |
| Grassland | 13,505.01 | 19.13 | 13,482.52 | 19.10 | 13,453.58 | 19.06 |
| Water | 79.9893 | 0.11 | 86.0904 | 0.12 | 105.2874 | 0.15 |
| Construction | 19.9017 | 0.03 | 24.0372 | 0.03 | 65.4102 | 0.09 |
| Unused | 55,902.14 | 79.19 | 55,669.04 | 78.86 | 55,476.72 | 78.59 |

Analysis of LULC Structure Change

Figure 4 shows the conversion relationship of the LULC for the three phases from 2000 to 2020, and it is represented visually by a chord diagram. The expansion of cropland and forest areas was obvious between 2000 and 2010. The expansion of cropland came mainly from the development of grassland and unused land, with a total increase of 95.14 $km^2$, while the forest area increased by 150.21 $km^2$, mainly from the evolution of grassland, and it was the only increase period of the three phases. During the time period of 2010–2020, the area of grassland transferred in was 2449.11 $km^2$ and the area transferred out was 2420.17 $km^2$. The overall area had increased, and the development of unused land had become an important way for grassland expansion to occur. The area of construction land doubled during this period, expanding much faster than in the previous period, while cropland was the main contributor to urban expansion, providing a total of 38.82 $km^2$ or 93.83% of the total. The area of forest shrank severely, with 64.62 $km^2$ of forest converted to unused land and 131.9 $km^2$ converted to grassland. From 2000 to 2020 as a whole, the main use types transferred out from the watershed were grassland and unused land, with 51.4323 $km^2$ and 425.428 $km^2$, respectively, being transferred out, and the use types transferred in were cropland, forest, and construction land, with 354.88 $km^2$, 51.17 $km^2$, and 45.50 $km^2$, respectively, being transferred in.

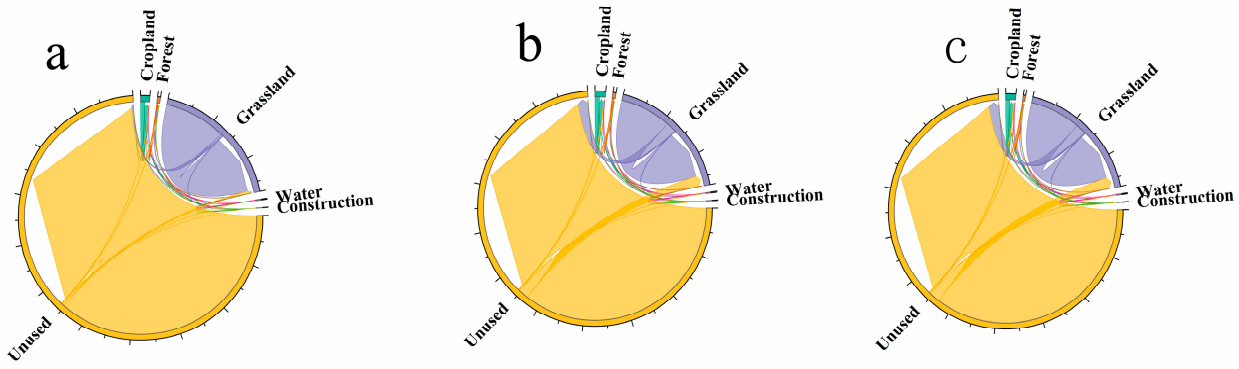


**Figure 4.** LULC transfer map of the KRB from 2000 to 2020. (**a**) 2000–2010; (**b**) 2010–2020; (**c**) 2000–2020.

*3.2. Spatiotemporal Variations in the LER in the KRB*

The LERI for the watershed had mean average values of 0.1721, 0.1714, and 0.1669 in 2000, 2010, and 2020, respectively. These values indicated a slight downward trend. Figure 5 shows that the LERI of the watershed had significant spatial and temporal variability. In the spatial distribution, the entire watershed was dominated by low and lower risks, while high and higher risks were mainly distributed along the Kriya River system, especially in the Daryaboyi, which are deep in the desert with sparse surrounding vegetation and poor natural conditions. The combined percentage of the study area's total area that was made up of the lowest risk and the lower risk was approximately constant, making up 98.69%,

97.88%, and 99.18% in 2000, 2010, and 2020, respectively. In 2000, 2010, and 2020, the total of the highest and highest risks is 0.29%, 0.58%, and 0.44%, respectively, with a slightly expanding and fluctuating trend towards the Northern Desert Region.

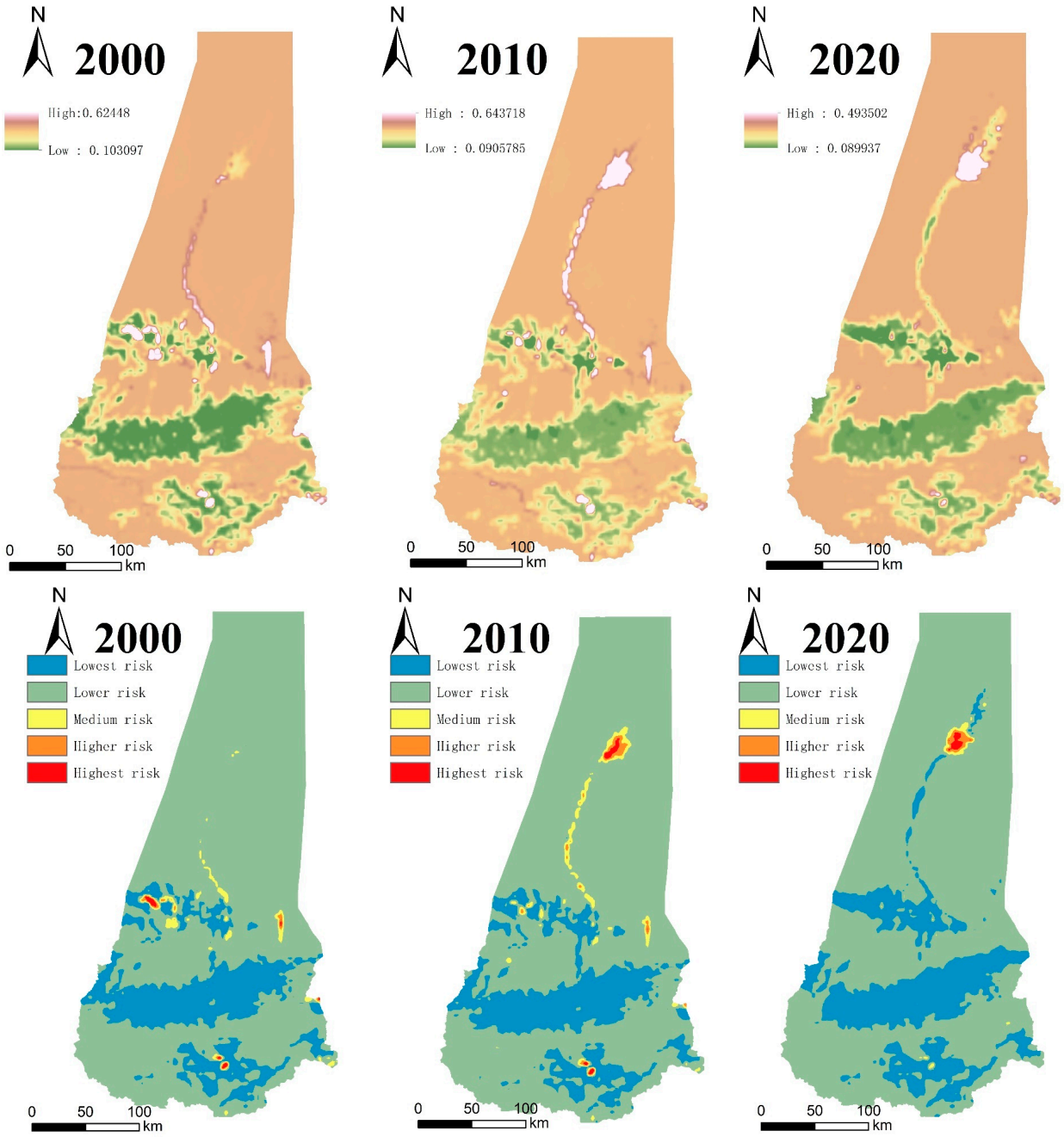


**Figure 5.** The spatially variable distribution of ERI in the KRB.

3.2.1. Defining the Temporal and Spatial Distribution of KRB

LER Moran's I values are, respectively, 0.818, 0.847, and 0.920 from 2000 to 2020 (Figure 6), all greater than 0.5. This indicated that the LERI of the KRB over the past 20 years had a positive and significant spatial correlation; in addition, the scattered points were distributed close to the regression line, suggests that the distribution of LER is spatially clustered and that this spatial clustering increases over time.

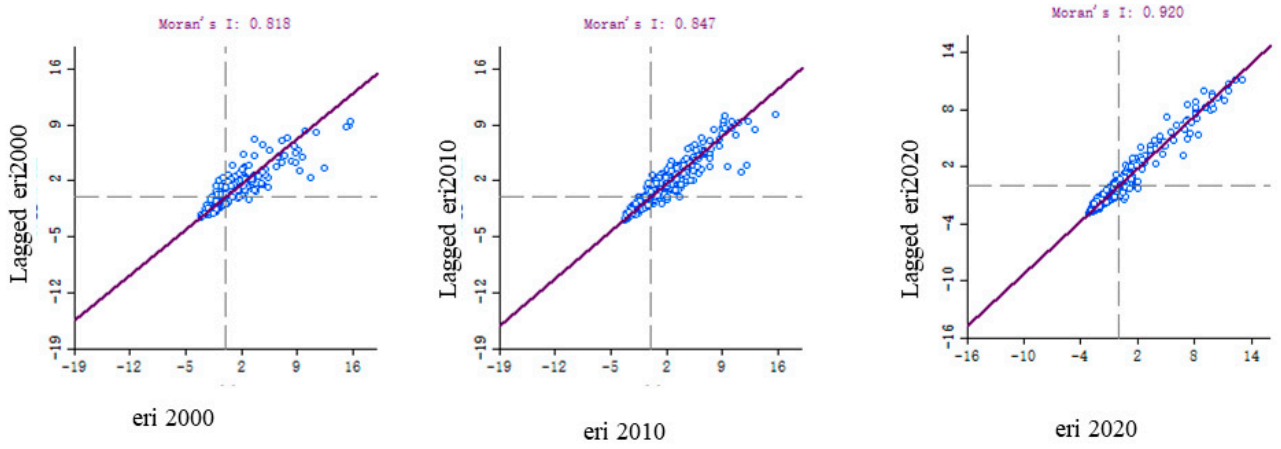


**Figure 6.** The ERI values in the KRB from 2000 to 2020 are shown in a scatter distribution of Moran's I index.

The trend of the LISA map for the period 2000 to 2020 (Figure 7) shows that the LER in the catchment area mainly has an aggregated "high–high" and "low–low" distribution. High-risk areas within the KRB exhibit concentration in the transition zone between desert and green land, particularly along the lower course of the Kriya River. These areas are characterized by pronounced landscape fragmentation. Additionally, sporadic high-risk areas are observed around the city. The high vegetation cover contributes to the relatively stable ecological quality, while low value zones are typically confined to grassland and cropland regions.

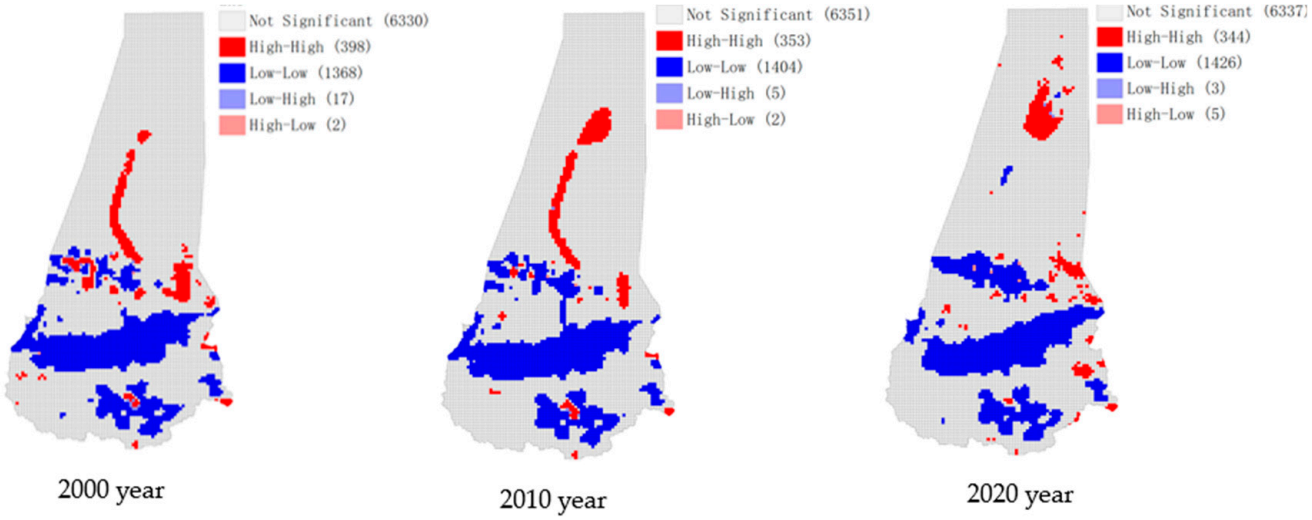


**Figure 7.** Map of the LISA clusters of the ERI in the KRB.

3.2.2. Analysis of Deriving Factor on the LER by the Geodetector Model

Based on factor detection, the LER of the KRB was examined with respect to the drivers for three periods from 2000 to 2020, and all factors passed the significance test ($p < 0.01$). Figure 8 displays the results of factor detection for each year. The LER of KRB is primarily driven by socioeconomic and natural condition factors, and each driving factor has a different contribution rate. For example, in 2000, soil conditions, annual temperature, precipitation, and DEM were the main influencing factors; in 2010, urban settlements, annual temperature, precipitation, and DEM were the dominant factors; and in 2020, GDP, population, annual temperature, and precipitation were the main influencing factors. According to the findings, environmental drivers will continue to have the greatest

influence on the spatial distribution of LER through the year 2020, while social drivers' influence will grow as society advances.

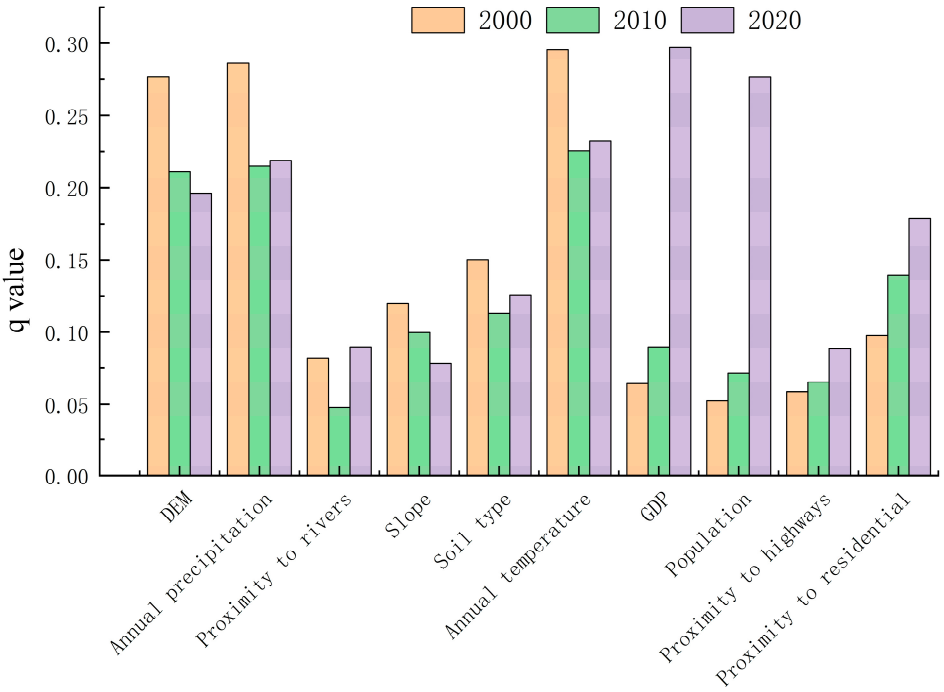


**Figure 8.** q-statistics of the factors influencing the changes in the ERI.

### *3.3. Multi-Scenario LULC and Multi-Scenario Modelling, 2030*

A comparison between the simulated and real LULC in 2020, together with the validation results and the spatial distribution of the PLUS model simulation error (Figure 9). With a Kappa coefficient of 0.818 and an FOM coefficient of 0.253, the PLUS model is generally more accurate. With its ability to accurately simulate variations in LULC demand within the KRB, the PLUS model shows a high degree of accuracy. This model provides a reliable foundation for future LER simulation predictions, enabling a more precise analysis of LER dynamics in response to LULC demand changes [13,58,59].

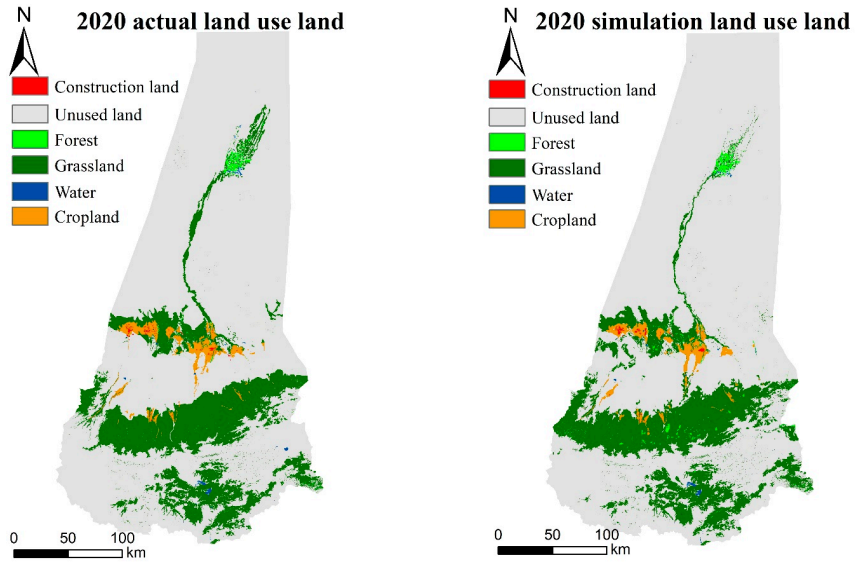


**Figure 9.** Actual and simulated land use types in the KRB for the year 2020.

### 3.3.1. Analysis of KRB Land Use While Modeling Multiple Scenarios

Figure 10 and Table 3 show the simulated LULC under different development scenarios for the year 2030, and they show different trends for each scenario for 2030 compared to the LULC for 2020. In accordance with Table 3, we can derive the following: (1) According to the NDS, compared to 2020, cropland, forest land, water, and construction land all increased. Forest land saw the largest increase, with a 92.83 km$^2$ increase, while grassland and unused land areas decreased. The construction land change rate was 60.37%. (2) Within the framework of CPS, the primary focus was on the protection of cropland. In this context, cropland witnessed a substantial increase in area, with a growth of 156.02 km$^2$ or 12.71%, representing the largest expansion among all types of land. The expansion of construction land, on the other hand, primarily resulted from the conversion of grassland and unused land. In comparison to the 2020 figures, the area of grassland decreased by 26.81 km$^2$, while the amount of construction land remained relatively stable. (3) Under the EPS: all ecological land areas increased to different degrees, including forest land, which increased by 66.27 km$^2$, and grassland, which increased by 132.48 km$^2$, and the total area of ecological land reached 13,918 km$^2$, which was the maximum area of ecological land under all scenarios.

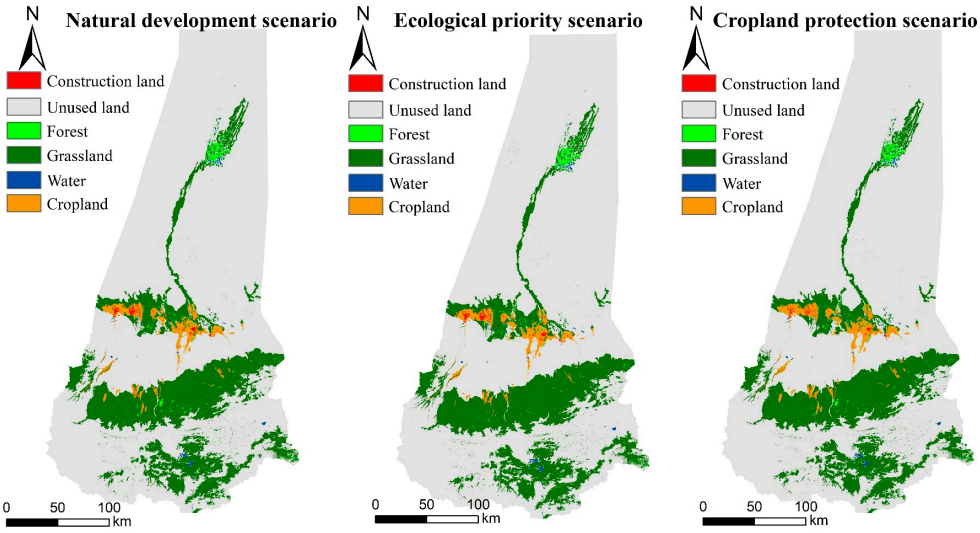


**Figure 10.** LULC under the different scenarios for the year 2030 in the KRB.

**Table 3.** Status of 2020 and Multi-scenario simulation of LULC change in 2030.

| | Scenario Type | Cropland/km$^2$ | Forest/km$^2$ | Grassland/km$^2$ | Water/km$^2$ | Construction Land/km$^2$ | Unused/km$^2$ |
|---|---|---|---|---|---|---|---|
| 2020 | | 1227.725 | 265.6377 | 13,453.58 | 105.2874 | 65.4102 | 55,476.72 |
| NDS | NDS | 1295.027 | 358.4763 | 13,449.61 | 111.4929 | 104.8995 | 55,274.85 |
| CPS | CPS | 1383.749 | 329.0373 | 13,426.77 | 111.4929 | 68.4603 | 55,274.85 |
| EPS | EPS | 1185.139 | 331.9137 | 13,586.06 | 111.4929 | 104.8995 | 55,274.85 |
| 2020–2030 | NDS | 5.48% | 34.95% | −0.03% | 5.89% | 60.37% | −0.36% |
| 2020–2031 | CPS | 12.71% | 23.87% | −0.20% | 5.89% | 4.66% | −0.36% |
| 2020–2032 | EPS | −3.47% | 24.95% | 0.98% | 5.89% | 60.37% | −0.36% |

### 3.3.2. Comparative Analysis of LER in Three Scenario Watersheds

Figure 11 depicts the spatial distribution of LER in the catchment in 2030 under various scenarios. Under NDS, CPS, and EPS conditions, respectively, the simulation yields an overall LERI for the catchment of 0.1682, 0.0933, and 0.0903, showing notable variations from those of 2020 (0.1669). The pattern distribution of LERI in the NDS scenario remains largely consistent with 2020. LERs decreased for both CPS and EPS. Comparing the overall spatial pattern distribution of LER, the similarity between the NDS and EPS was extremely high compared to that of 2020, while the lower risk occupied a very large area in the arable

CPS, and the lower risk dominated. In addition, the map clearly showed that ecological land was located in areas with low levels of LER, such as grassland and forest areas. High-risk areas in Daryabuyi under different scenarios in 2030. Combined with Figure 12, the ecological risk ratio of the landscape for 2020 and 2030 under each scenario showed that low risk and lower risk were always in the dominant position, but the area of each ecological risk zone under the different scenarios was still significantly different, especially in the 2030 arable land protection scenario where the low-risk zone accounted for 99.1%. It is also worth mentioning that the largest area of high-risk zone was in 2020, reaching 116.899 km$^2$, which indicated that there were many ecological risks in the current LULC.

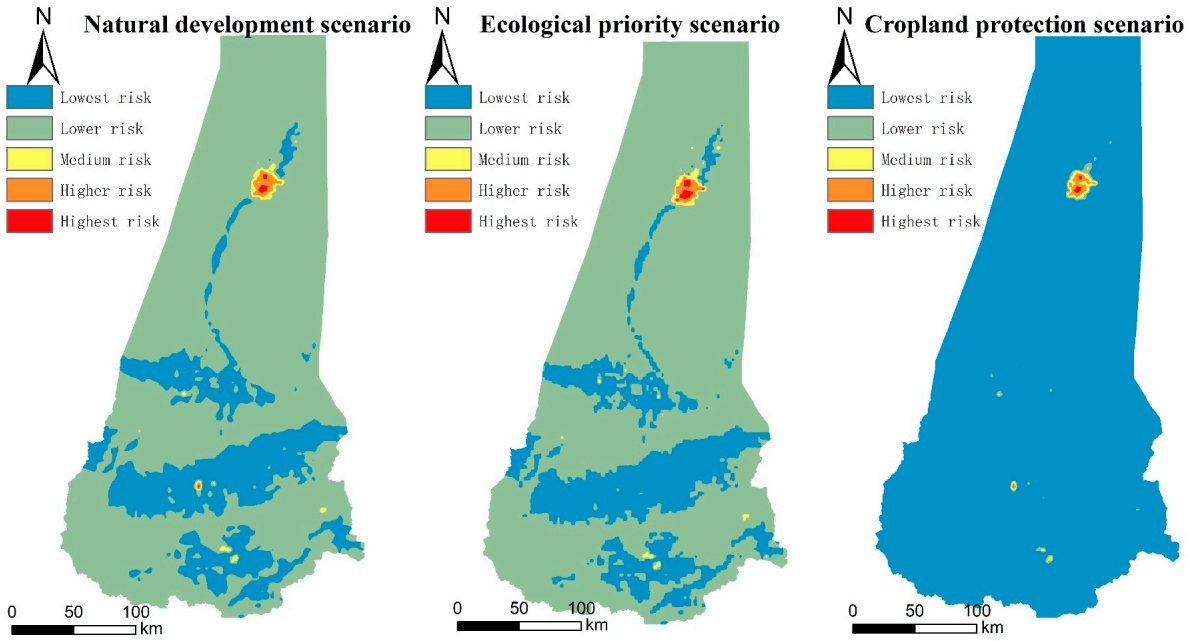


**Figure 11.** Spatial patterns of the LER rankings in the KRB under the different scenarios for the year 2030.

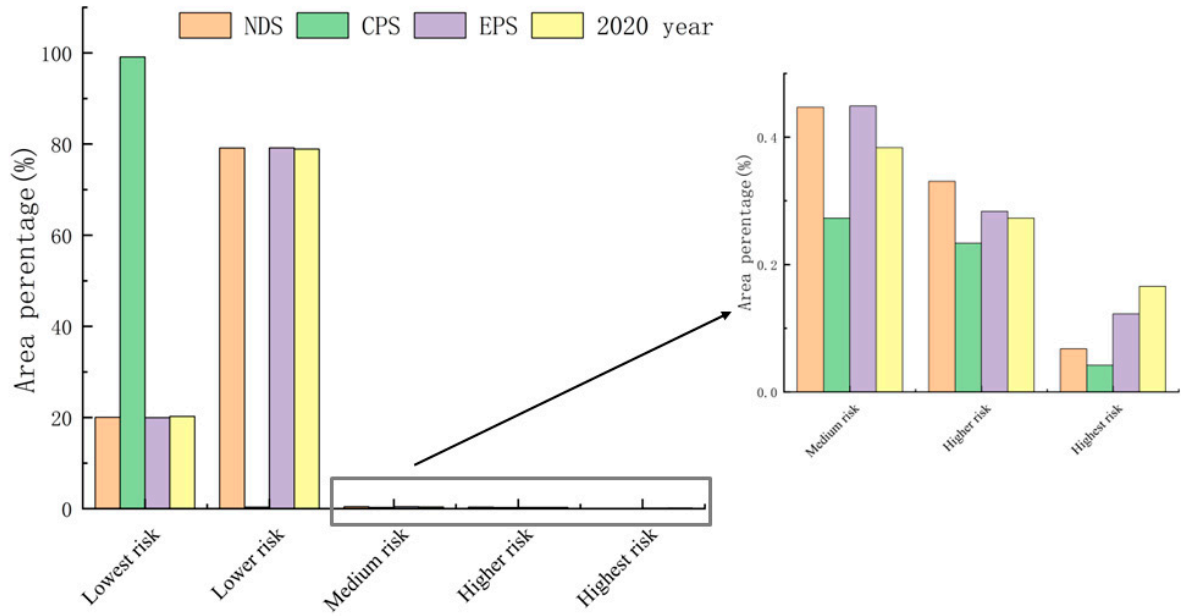


**Figure 12.** Percentage of area in the ecological risk class of the KRB landscape under different scenarios.

## 4. Discussion

### *4.1. The KRB Shows a Spatial Distribution of ERI*

Spatial and temporal variations in ecological risk in arid zone watersheds are negative manifestations of natural and social impacts, and LERI can reflect the degree to which watershed ecosystems are threatened by climate change and human activities, thereby revealing mechanisms and trends in ecological processes [60,61]. With LULC serving as a driving force, we found a connection between LER patterns, offering a way to examine the temporal and spatial dynamics of LER. It was discovered that during the period of 2000–2020, the spatial and temporal distribution characteristics of LER in the KRB changed more, primarily in the following ways: Prior to 2010, the area of cultivated land in the central part of the basin was primarily where the high and higher risks were concentrated. This is mainly because the study area is constrained by climatic and environmental factors, the KRB is located in the Gobi Desert, which is arid with low rainfall, and water resource constraints are obvious. This, coupled with the rapid development of agriculture which has led to a large amount of water resource depletion, and because the arable land has been distributed in a fragmented manner, has resulted in poorer landscape connectivity and a relatively high level of ecological risk. The overall LER in the catchment shows a decreasing trend after 2010, with a significant decrease in high-risk areas and an increase in the proportion of low- and medium-risk areas, although there has been an increase in ecologically risky areas in Dariyaboi due to the displacement of downstream water use by upstream water use for irrigated agriculture. In an effort to address the declining ecological environment, the Chinese government has started to restore farmland to forests and grasslands [53,62,63], which to some extent improves the ecological quality and reduces the probability of land degradation, as evidenced by the area of forest the past 20 years.

### *4.2. Impacts of the Driving Factors on the Pattern of the LER*

Taking into account the unique natural geographical, climatic, and social conditions of the KRB, this study explored the intrinsic mechanisms of the LER changes from the perspective of socioeconomic and natural factors. The geodetector results showed significant differences in the main drivers of the LER changes for the three phases from 2000 to 2020. The 20-year period from the initial temperature, precipitation, and topography-driven factors to the GDP, population, temperature, and residence area factors in 2020 showed a very high influence; this indicates, to some extent, that human activities have become an important part of influencing the LER. The period 2000–2020 was a period of rapid economic development from the perspective of the GDP. The 11-fold increase in GDP in the KRB during the two periods was directly manifested by the large expansion in land for construction and was based on encroachment on arable land. However, the increase in the population increased the exploitation and excavation of resources, which was clearly expressed through the expansion in arable land [17,64]. Agriculture and animal husbandry were the main sources of GDP in the basin, and during the study period, regarding the population and socioeconomic development, people increased the area of arable land, which resulted in a large amount of resource plundering in rivers as well as surrounding water bodies, leading to the degradation of the original grassland and artificially changing the spatial configuration of water resources in the basin, which seriously damaged the ecological water use and degraded the grassland vegetation without any resupply [9,65]. Combined with the spatial characteristics of the LER, the locations of the grassland had substantial impacts on the LERs of the watershed areas, and the total area of grassland in 2020 did not change much compared to 2010, but the area of grassland on both sides of the Kriya channel in 2020 increased significantly; that is, this change made the LER of the whole watershed decrease, and the landscape pattern played a key role in relation to the LER.

### *4.3. Creation of Future LULC Policies and LER Administration*

In the KRB region, both natural and societal factors predominantly dictate changes in land use resources, with the natural environment forming the foundational basis that invariably experiences impacts during economic development [66]. Concurrently, amidst the backdrop of severe global climatic alterations, arid zone climates have transitioned from "warm–humid" to "warm–dry" [67]. This shift, coupled with heightened evaporation from river basins, has strained the balance between water resource supply and demand. The land use/cover and landscape patterns in the KRB have drastically transformed over the past two decades [49,68,69]. As the climate in the watershed has evolved, there has been an upsurge in glacial snowmelt runoff upstream, thereby enhancing the accessibility of water resources for agricultural production in the midstream region [70]. However, the expanding cultivated land area in the midstream region, driven by agricultural economic activities, has considerably elevated the demand for agricultural water. Concurrently, the large-scale development of arable land has substantially altered the landscape pattern of natural vegetation in the mid and downstream areas of the river. This alteration has influenced the ecological water demand of the vegetation, leading to a more noticeable trend of vegetation degradation. The rising demand for agricultural water and the decreasing ecological water demand of vegetation have significantly altered the water demand structure of the river basin, as evident in the spatial distribution of the high-risk area of LER from 2000 to 2020. The key ecological LULC in the KRB region is grassland, which, compared to other areas, displays heightened susceptibility and plays a critical role in mitigating ecological risks [9,36].

To safeguard grasslands, moderate grazing intensities can enhance their resilience and bolster their habitat quality stability in riverine ecosystems. Reducing watershed LER necessitates diverse strategies, contingent on the specific region: (1) In high-risk areas, meticulous consideration of natural conditions and actual economic needs is crucial. One strategy involves accommodating the demand for ecological land through natural restoration, encompassing comprehensive protection of forests, grasslands, and arable land, and strategic planning to resolve the conflict between ecological and economic water usage. This includes proactive ecological restoration efforts and the conversion of farmland back to forests and grasslands. Simultaneously, it is essential to develop the agricultural economy in alignment with local conditions, advocate for energy- and water-efficient agricultural management models, and encourage agricultural restructuring. (2) Recognizing the evident spatial variation of LER, adjustments to the spatial distribution pattern of LULC can be employed as a component of ecological risk management. In areas characterized by concentrated ecological risks, it is crucial to address landscape fragmentation and employ spatial governance strategies at the national level. This should entail implementing regionally specific control measures that are tailored to the local natural conditions.

### *4.4. Limitations and Future Work*

In this investigation, an analysis of the Land Ecological Risk (LER) status within the Kriya River Basin (KRB) over the past two decades was undertaken, employing a landscape ecology perspective. The study aimed to elucidate the spatial and temporal distribution of LER while investigating the mechanisms of influencing factors on ecological risk. Furthermore, the research extended to designing and simulating ecological risks under different development scenarios projected for the year 2030. The overarching objective was to provide a theoretical foundation for future ecological risk control measures. Arid zone watersheds, characterized by ecologically sensitive attributes, have witnessed a surge in ecological issues in recent years [2,11]. These concerns have manifested as typical ecological and environmental problems observed globally, garnering extensive attention from various sectors of society. Consequently, the development of a rational and effective ecological assessment model for watersheds, especially those with unique natural geographical conditions like the KRB, assumes critical importance. In this paper, a landscape pattern

index was formulated based on land use (LULC) data to assess the KRB. This method proves feasible for managing land resources within the basin and addressing regional ecological and environmental challenges. However, the study acknowledges certain limitations owing to the intricate nature of data sources and ecological risks in the area. The uncertainties introduced as a result of these complexities impact the outcomes of the comprehensive assessment. Notably, the risk assessment method grounded in landscape ecology exhibits a discernible scale effect, where the size of the scale influences the calculation results of the landscape pattern index, leading to potential bias [17,35]. Additionally, the driving factors behind changes in land use landscape patterns within the KRB are exceedingly intricate. The selection of some natural and anthropogenic factors in this study, while omitting others challenging to quantify, hinders the precise prediction of the future spatial pattern of land use in the simulation. Subsequent research endeavors should consider a multi-scale comprehensive assessment, emphasizing the scale effects of diverse influencing factors for a more accurate evaluation. Furthermore, exploring additional quantitative driving analysis indicators in conjunction with the specific conditions of the KRB will contribute to enhancing the simulation's accuracy.

## 5. Conclusions

This study employs the Landscape Ecological Risk Assessment (LERA) model to conduct a comprehensive examination of the spatial and temporal dynamics within the Kriya River Basin (KRB) from 2000 to 2020. Additionally, the investigation integrates the PLUS model to simulate and forecast the spatial distribution of LER, projecting potential trends in the KRB under diverse scenarios by the year 2030. (1) The KRB predominantly encompasses grassland and unused land, constituting over 97% of its total expanse. Over the two-decade timeframe, notable expansions occur in cropland, water, and construction land, while unused land and grassland witness contractions. Spatial alterations notably reveal that the proliferation of construction land predominantly encroaches upon cropland. (2) The period from 2000 to 2020 manifests a discernible spatial clustering pattern of Ecological Risk Index (ERI) values in the KRB, with an observed escalation in the degree of clustering. Dominating the LER spectrum are low-ecological-risk areas and lower-ecological-risk areas. (3) ERI, as an index, reflects the confluence of socioeconomic and natural conditions, and its principal determinants undergo a nuanced transition over the two decades. In the early 2000s, natural variables including temperature, precipitation, topography, and soil type wield substantial influence, whereas by 2020, socioeconomic factors such as GDP, population, temperature, topography, and proximity to settlements emerge as predominant factors shaping LER. Human activities progressively assert themselves as the paramount catalyst for LER variations. (4) The anticipated landscape configurations under three distinct KRB scenarios in 2030 portray varied degrees of transformation, wherein low-risk and high-risk areas predominate within the NDS, CPS, and EPS scenarios. Spatially, high-risk LERs exhibit notable concentration, particularly evident in the Daryabuyi site across divergent scenarios. The conclusions of the study can provide a decision-making basis for ecological risk early warning for the ecological protection of the Kriya River Basin, enhancement of the ecological security level as well as giving full play to the role of ecological functional zones of inland river basins in arid zones.

**Author Contributions:** Conceptualization, J.L.; methodology, J.L.; software, X.H. validation, R.W.; writing—original draft, J.L.; resources, P.H., Z.W. and R.W.; project management, X.H.; Funding acquisition, X.H. All authors have read and agreed to the published version of the manuscript.

**Funding:** This research was funded by the National Science Foundation of China (grant no. 41975115) and research on ecological dispatch and ecological response in the Kriya River Basin (grant no. 2020.B-003).

**Data Availability Statement:** No new data were created or analyzed in this study. Data sharing is not applicable to this article.

**Acknowledgments:** We are very reviewers for their comments on the paper revision. We would also like to thank Li Xu and Yanqiu Chen for their comments on the model and paper revisions in.

**Conflicts of Interest:** The authors declare no conflict of interest.

## References


1. He, S.; Wang, D.; Zhao, P.; Li, Y.; Lan, H.; Chen, W.; Chen, X. Quantification of basin-scale multiple ecosystem services in ecologically fragile areas. *Catena* **2021**, *202*, 105247. [CrossRef]
2. Wang, J.; Wu, Y.; Hu, Z.; Zhang, J. Remote Sensing of Watershed: Towards a New Research Paradigm. *Remote Sens.* **2023**, *15*, 2569. [CrossRef]
3. Zhang, H.; Xue, L.; Wei, G.; Dong, Z.; Meng, X. Assessing Vegetation Dynamics and Landscape Ecological Risk on the Mainstream of Tarim River, China. *Water* **2020**, *12*, 2156. [CrossRef]
4. Wang, J.; Zhen, J.; Hu, W.; Chen, S.; Lizaga, I.; Zeraatpisheh, M.; Yang, X. Remote sensing of soil degradation: Progress and perspective. *Int. Soil Water Conserv. Res.* **2023**, *11*, 429–454. [CrossRef]
5. Li, S.; Zhang, J.; Guo, E.; Zhang, F.; Ma, Q.; Mu, G. Dynamics and ecological risk assessment of chromophoric dissolved organic matter in the Yinma River Watershed: Rivers, reservoirs, and urban waters. *Environ. Res.* **2017**, *158*, 245–254. [CrossRef]
6. Ferreira, A.R.L.; Sanches Fernandes, L.F.; Cortes, R.M.V.; Pacheco, F.A.L. Assessing anthropogenic impacts on riverine ecosystems using nested partial least squares regression. *Sci. Total Environ.* **2017**, *583*, 466–477. [CrossRef]
7. Wang, J.; Ding, J.; Yu, D.; Ma, X.; Zhang, Z.; Ge, X.; Teng, D.; Li, X.; Liang, J.; Lizaga, I.; et al. Capability of Sentinel-2 MSI data for monitoring and mapping of soil salinity in dry and wet seasons in the Ebinur Lake region, Xinjiang, China. *Geoderma* **2019**, *353*, 172–187. [CrossRef]
8. Dupras, J.; Marull, J.; Parcerisas, L.; Coll, F.; Gonzalez, A.; Girard, M.; Tello, E. The impacts of urban sprawl on ecological connectivity in the Montreal Metropolitan Region. *Environ. Sci. Policy* **2016**, *58*, 61–73. [CrossRef]
9. Gan, L.; Halik, Ü.; Shi, L.; Welp, M. Ecological risk assessment and multi-scenario dynamic prediction of the arid oasis cities in northwest China from 1990 to 2030. *Stoch. Environ. Res. Risk Assess.* **2023**, *37*, 3099–3115. [CrossRef]
10. Aguilera, M.A.; González, M.G. Urban infrastructure expansion and artificial light pollution degrade coastal ecosystems, increasing natural-to-urban structural connectivity. *Landsc. Urban Plan.* **2023**, *229*, 104609. [CrossRef]
11. Wang, J.; Ding, J.; Li, G.; Liang, J.; Yu, D.; Aishan, T.; Zhang, F.; Yang, J.; Abulimiti, A.; Liu, J. Dynamic detection of water surface area of Ebinur Lake using multi-source satellite data (Landsat and Sentinel-1A) and its responses to changing environment. *Catena* **2019**, *177*, 189–201. [CrossRef]
12. Hou, M.; Ge, J.; Gao, J.; Meng, B.; Li, Y.; Yin, J.; Liu, J.; Feng, Q.; Liang, T. Ecological Risk Assessment and Impact Factor Analysis of Alpine Wetland Ecosystem Based on LUCC and Boosted Regression Tree on the Zoige Plateau, China. *Remote Sens.* **2020**, *12*, 368. [CrossRef]
13. Li, W.; Lin, Q.; Hao, J.; Wu, X.; Zhou, Z.; Lou, P.; Liu, Y. Landscape Ecological Risk Assessment and Analysis of Influencing Factors in Selenga River Basin. *Remote Sens.* **2023**, *15*, 4262. [CrossRef]
14. Malekmohammadi, B.; Rahimi Blouchi, L. Ecological risk assessment of wetland ecosystems using Multi Criteria Decision Making and Geographic Information System. *Ecol. Indic.* **2014**, *41*, 133–144. [CrossRef]
15. Mo, W.; Wang, Y.; Zhang, Y.; Zhuang, D. Impacts of road network expansion on landscape ecological risk in a megacity, China: A case study of Beijing. *Sci. Total Environ.* **2017**, *574*, 1000–1011. [CrossRef] [PubMed]
16. Liu, J.; Kuang, W.; Zhang, Z.; Xu, X.; Qin, Y.; Ning, J.; Zhou, W.; Zhang, S.; Li, R.; Yan, C.; et al. Spatiotemporal characteristics, patterns, and causes of land-use changes in China since the late 1980s. *J. Geogr. Sci.* **2014**, *24*, 195–210. [CrossRef]
17. Du, L.; Dong, C.; Kang, X.; Qian, X.; Gu, L. Spatiotemporal evolution of land cover changes and landscape ecological risk assessment in the Yellow River Basin, 2015–2020. *J. Environ. Manag.* **2023**, *332*, 117149. [CrossRef]
18. Song, Q.; Hu, B.; Peng, J.; Bourennane, H.; Biswas, A.; Opitz, T.; Shi, Z. Spatio-temporal variation and dynamic scenario simulation of ecological risk in a typical artificial oasis in northwestern China. *J. Clean. Prod.* **2022**, *369*, 133302. [CrossRef]
19. Ma, J.; Yu, Q.; Wang, H.; Yang, L.; Wang, R.; Fang, M. Construction and Optimization of Wetland Landscape Ecological Network in Dongying City, China. *Land* **2022**, *11*, 1226. [CrossRef]
20. Qian, Y.; Dong, Z.; Yan, Y.; Tang, L. Ecological risk assessment models for simulating impacts of land use and landscape pattern on ecosystem services. *Sci. Total Environ.* **2022**, *833*, 155218. [CrossRef]
21. Lan, J.; Chai, Z.; Tang, X.; Wang, X. Landscape Ecological Risk Assessment and Driving Force Analysis of the Heihe River Basin in the Zhangye Area of China. *Water* **2023**, *15*, 3588. [CrossRef]
22. Li, W.; Wang, Y.; Xie, S.; Sun, R.; Cheng, X. Impacts of landscape multifunctionality change on landscape ecological risk in a megacity, China: A case study of Beijing. *Ecol. Indic.* **2020**, *117*, 106681. [CrossRef]
23. Li, S.; He, W.; Wang, L.; Zhang, Z.; Chen, X.; Lei, T.; Wang, S.; Wang, Z. Optimization of landscape pattern in China Luojiang Xiaoxi basin based on landscape ecological risk assessment. *Ecol. Indic.* **2023**, *146*, 109887. [CrossRef]
24. Zhao, Y.; Tao, Z.; Wang, M.; Chen, Y.; Wu, R.; Guo, L. Landscape Ecological Risk Assessment and Planning Enlightenment of Songhua River Basin Based on Multi-Source Heterogeneous Data Fusion. *Water* **2022**, *14*, 4060. [CrossRef]
25. Li, H.; Su, F.; Guo, C.; Dong, L.; Song, F.; Wei, C.; Zheng, Y. Landscape ecological risk assessment and driving mechanism of coastal estuarine tidal flats—A case study of the liaohe estuary wetlands. *Front. Environ. Sci.* **2022**, *10*, 2417. [CrossRef]

26. Wang, G.; Ran, G.; Chen, Y.; Zhang, Z. Landscape Ecological Risk Assessment for the Tarim River Basin on the Basis of Land-Use Change. *Remote Sens.* **2023**, *15*, 4173. [CrossRef]
27. Li, J.; Pu, R.; Gong, H.; Luo, X.; Ye, M.; Feng, B. Evolution Characteristics of Landscape Ecological Risk Patterns in Coastal Zones in Zhejiang Province, China. *Sustainability* **2017**, *9*, 584. [CrossRef]
28. De Montis, A.; Caschili, S.; Mulas, M.; Modica, G.; Ganciu, A.; Bardi, A.; Ledda, A.; Dessena, L.; Laudari, L.; Fichera, C.R. Urban–rural ecological networks for landscape planning. *Land Use Policy* **2016**, *50*, 312–327. [CrossRef]
29. Heggem, D.T.; Edmonds, C.M.; Neale, A.C.; Bice, L.; Jones, K.B. A Landscape Ecology Assessment of the Tensas River Basin. *Environ. Monit. Assess.* **2000**, *64*, 41–54. [CrossRef]
30. Kapustka, L.A.; Galbraith, H.; Luxon, B.M.; Yocum, J. Using landscape ecology to focus ecological risk assessment and guide risk management decision-making. *Toxicol. Ind. Health* **2001**, *17*, 236–246. [CrossRef]
31. Paukert, C.P.; Pitts, K.L.; Whittier, J.B.; Olden, J.D. Development and assessment of a landscape-scale ecological threat index for the Lower Colorado River Basin. *Ecol. Indic.* **2011**, *11*, 304–310. [CrossRef]
32. Karimian, H.; Zou, W.; Chen, Y.; Xia, J.; Wang, Z. Landscape ecological risk assessment and driving factor analysis in Dongjiang river watershed. *Chemosphere* **2022**, *307*, 135835. [CrossRef] [PubMed]
33. Zhou, Z.; Zhao, W.; Lv, S.; Huang, D.; Zhao, Z.; Sun, Y. Spatiotemporal Transfer of Source-Sink Landscape Ecological Risk in a Karst Lake Watershed Based on Sub-Watersheds. *Land* **2023**, *12*, 1330. [CrossRef]
34. Pan, N.; Guan, Q.; Wang, Q.; Sun, Y.; Li, H.; Ma, Y. Spatial Differentiation and Driving Mechanisms in Ecosystem Service Value of Arid Region: A case study in the middle and lower reaches of Shule River Basin, NW China. *J. Clean. Prod.* **2021**, *319*, 128718. [CrossRef]
35. Lin, X.; Wang, Z. Landscape ecological risk assessment and its driving factors of multi-mountainous city. *Ecol. Indic.* **2023**, *146*, 109823. [CrossRef]
36. Hou, Y.; Chen, Y.; Li, Z.; Li, Y.; Sun, F.; Zhang, S.; Wang, C.; Feng, M. Land Use Dynamic Changes in an Arid Inland River Basin Based on Multi-Scenario Simulation. *Remote Sens.* **2022**, *14*, 2797. [CrossRef]
37. Gong, J.; Zhao, C.-X.; Xie, Y.-C.; Gao, Y.-J. Ecological risk assessment and its management of Bailongjiang watershed, southern Gansu based on landscape pattern. *Yingyong Shengtai Xuebao* **2014**, *25*, 2041–2048.
38. Shi, Y.; Wang, R.; Lu, Y.; Song, S.; Johnson, A.C.; Sweetman, A.; Jones, K. Regional multi-compartment ecological risk assessment: Establishing cadmium pollution risk in the northern Bohai Rim, China. *Environ. Int.* **2016**, *94*, 283–291. [CrossRef]
39. Wang, W.; Wang, H.; Zhou, X. Ecological risk assessment of watershed economic zones on the landscape scale: A case study of the Yangtze River Economic Belt in China. *Reg. Environ. Chang.* **2023**, *23*, 105. [CrossRef]
40. Islam, K.; Rahman, M.F.; Jashimuddin, M. Modeling land use change using Cellular Automata and Artificial Neural Network: The case of Chunati Wildlife Sanctuary, Bangladesh. *Ecol. Indic.* **2018**, *88*, 439–453. [CrossRef]
41. Albert, C.H.; Hervé, M.; Fader, M.; Bondeau, A.; Leriche, A.; Monnet, A.-C.; Cramer, W. What ecologists should know before using land use/cover change projections for biodiversity and ecosystem service assessments. *Reg. Environ. Chang.* **2020**, *20*, 106. [CrossRef]
42. Zhou, M.; Ma, Y.; Tu, J.; Wang, M. SDG-oriented multi-scenario sustainable land-use simulation under the background of urban expansion. *Env. Sci. Pollut. Res. Int.* **2022**, *29*, 72797–72818. [CrossRef] [PubMed]
43. Gao, B.; Wu, Y.; Li, C.; Zheng, K.; Wu, Y.; Wang, M.; Fan, X.; Ou, S. Multi-Scenario Prediction of Landscape Ecological Risk in the Sichuan-Yunnan Ecological Barrier Based on Terrain Gradients. *Land* **2022**, *11*, 2079. [CrossRef]
44. Darvishi, A.; Yousefi, M.; Marull, J. Modelling landscape ecological assessments of land use and cover change scenarios. Application to the Bojnourd Metropolitan Area (NE Iran). *Land Use Policy* **2020**, *99*, 105098. [CrossRef]
45. Huang, D.; Huang, J.; Liu, T. Delimiting urban growth boundaries using the CLUE-S model with village administrative boundaries. *Land Use Policy* **2019**, *82*, 422–435. [CrossRef]
46. Liu, X.; Liang, X.; Li, X.; Xu, X.; Ou, J.; Chen, Y.; Li, S.; Wang, S.; Pei, F. A future land use simulation model (FLUS) for simulating multiple land use scenarios by coupling human and natural effects. *Landsc. Urban Plan.* **2017**, *168*, 94–116. [CrossRef]
47. Liang, X.; Guan, Q.; Clarke, K.C.; Liu, S.; Wang, B.; Yao, Y. Understanding the drivers of sustainable land expansion using a patch-generating land use simulation (PLUS) model: A case study in Wuhan, China. *Comput. Environ. Urban Syst.* **2021**, *85*, 101569. [CrossRef]
48. Wang, J.; Zhang, F.; Luo, G.; Guo, Y.; Zheng, J.; Wu, S.; Wang, D.; Liu, S.; Shi, Q. Factors Influencing Seasonal Changes in Inundation of the Daliyaboyi Oasis, Lower Keriya River Valley, Central Tarim Basin, China. *Remote Sens.* **2022**, *14*, 5050. [CrossRef]
49. Muyibul, Z.; Jianxin, X.; Muhtar, P.; Qingdong, S.; Run, Z. Spatiotemporal changes of land use/cover from 1995 to 2015 in an oasis in the middle reaches of the Keriya River, southern Tarim Basin, Northwest China. *Catena* **2018**, *171*, 416–425. [CrossRef]
50. Sun, N.S.; Chen, Q.; Liu, F.G.; Zhou, Q.; He, W.X.; Guo, Y.Y. Land Use Simulation and Landscape Ecological Risk Assessment on the Qinghai-Tibet Plateau. *Land* **2023**, *12*, 923. [CrossRef]
51. Lin, Y.; Hu, X.; Zheng, X.; Hou, X.; Zhang, Z.; Zhou, X.; Qiu, R.; Lin, J. Spatial variations in the relationships between road network and landscape ecological risks in the highest forest coverage region of China. *Ecol. Indic.* **2019**, *96*, 392–403. [CrossRef]
52. Li, C.; Chen, J.; Liao, M.; Chen, G.; Zhou, Q. Ecological Risk Assessment of Shan Xin Mining Area Based on Remote Sensing and Geography Information System Technology. *J. Geogr. Inf. Syst.* **2018**, *10*, 234–246. [CrossRef]

53. Zhang, T.; Du, Z.; Yang, J.; Yao, X.; Ou, C.; Niu, B.; Yan, S. Land Cover Mapping and Ecological Risk Assessment in the Context of Recent Ecological Migration. *Remote Sens.* **2021**, *13*, 1381. [CrossRef]
54. Wang, S.; Tan, X.; Fan, F. Landscape Ecological Risk Assessment and Impact Factor Analysis of the Qinghai–Tibetan Plateau. *Remote Sens.* **2022**, *14*, 4726. [CrossRef]
55. Huang, X.; Wang, X.; Zhang, X.; Zhou, C.; Ma, J.; Feng, X. Ecological risk assessment and identification of risk control priority areas based on degradation of ecosystem services: A case study in the Tibetan Plateau. *Ecol. Indic.* **2022**, *141*, 109078. [CrossRef]
56. Wang, J.-F.; Hu, Y. Environmental health risk detection with GeogDetector. *Environ. Model. Softw.* **2012**, *33*, 114–115. [CrossRef]
57. Fu, F.; Deng, S.; Wu, D.; Liu, W.; Bai, Z. Research on the spatiotemporal evolution of land use landscape pattern in a county area based on CA-Markov model. *Sustain. Cities Soc.* **2022**, *80*, 103760. [CrossRef]
58. Zhang, Z.; Hu, B.; Jiang, W.; Qiu, H. Identification and scenario prediction of degree of wetland damage in Guangxi based on the CA-Markov model. *Ecol. Indic.* **2021**, *127*, 107764. [CrossRef]
59. Zhang, S.; Chen, C.; Yang, Y.; Huang, C.; Wang, M.; Tan, W. Coordination of economic development and ecological conservation during spatiotemporal evolution of land use/cover in eco-fragile areas. *Catena* **2023**, *226*, 107097. [CrossRef]
60. Preuss, T.G.; Hommen, U.; Alix, A.; Ashauer, R.; van den Brink, P.; Chapman, P.; Ducrot, V.; Forbes, V.; Grimm, V.; Schafer, D.; et al. Mechanistic effect models for ecological risk assessment of chemicals (MEMoRisk)-a new SETAC-Europe Advisory Group. *Environ. Sci. Pollut. Res.* **2009**, *16*, 250–252. [CrossRef]
61. Chen, L.; Sun, R.; Lu, Y. A conceptual model for a process-oriented landscape pattern analysis. *Sci. China Earth Sci.* **2019**, *62*, 2050–2057. [CrossRef]
62. Bennett, M.T. China's sloping land conversion program: Institutional innovation or business as usual? *Ecol. Econ.* **2008**, *65*, 699–711. [CrossRef]
63. Xu, J.; Yin, R.; Li, Z.; Liu, C. China's ecological rehabilitation: Unprecedented efforts, dramatic impacts, and requisite policies. *Ecol. Econ.* **2006**, *57*, 595–607. [CrossRef]
64. Liu, Z.; Liu, Y.; Wang, J. A global analysis of agricultural productivity and water resource consumption changes over cropland expansion regions. *Agric. Ecosyst. Environ.* **2021**, *321*, 107630. [CrossRef]
65. Yu, Y.; Yu, R.; Chen, X.; Yu, G.; Gan, M.; Disse, M. Agricultural water allocation strategies along the oasis of Tarim River in Northwest China. *Agric. Water Manag.* **2017**, *187*, 24–36. [CrossRef]
66. Ponce-Campos, G.E.; Moran, M.S.; Huete, A.; Zhang, Y.; Bresloff, C.; Huxman, T.E.; Eamus, D.; Bosch, D.D.; Buda, A.R.; Gunter, S.A.; et al. Ecosystem resilience despite large-scale altered hydroclimatic conditions. *Nature* **2013**, *494*, 349–352. [CrossRef] [PubMed]
67. Yao, J.; Chen, Y.; Guan, X.; Zhao, Y.; Chen, J.; Mao, W. Recent climate and hydrological changes in a mountain–basin system in Xinjiang, China. *Earth-Sci. Rev.* **2022**, *226*, 103957. [CrossRef]
68. Wang, R.; Zayit, A.; He, X.; Han, D.; Yang, G.; Lv, G. Ecological Water Requirement of Vegetation and Water Stress Assessment in the Middle Reaches of the Keriya River Basin. *Remote Sens.* **2023**, *15*, 4638. [CrossRef]
69. Yan, W.; Wang, Y.; Ma, X.; Liu, M.; Yan, J.; Tan, Y.; Liu, S. Snow Cover and Climate Change and Their Coupling Effects on Runoff in the Keriya River Basin during 2001–2020. *Remote Sens.* **2023**, *15*, 3435. [CrossRef]
70. Jiang, N.; Zhang, Q.; Zhang, S.; Zhao, X.; Cheng, H. Spatial and temporal evolutions of vegetation coverage in the Tarim River Basin and their responses to phenology. *Catena* **2022**, *217*, 106489. [CrossRef]